ADVANCEMENTS IN MILLIMETER WAVE TELESCOPE PANEL FABRICATION

by

Zack Hatfield

A Masters Report Submitted to the Faculty of the

JAMES C. WYANT COLLEGE OF OPTICAL SCIENCES

In Partial Fulfillment of the Requirements

For the Degree of

MASTER OF SCIENCE

In the Graduate College

THE UNIVERSITY OF ARIZONA

2021

Acknowledgements

I would like to start by thanking everyone who has helped me along the way throughout my academic and research career, including all the professors and TAs who taught me many things, and my research colleagues who worked with me to generate much of what will be presented in this report.

Firstly, to all my colleagues at the Steward Observatory Solar Lab and the Large Optics Fabrication and Testing Group, for their consistent support and friendship as we tackle challenging problems and continue to learn together.

Special thanks go to Justin Hyatt for leading the thermoforming team effort, introducing me to the world of research, teaching me how to be creative and practical in the way I approach engineering problems, and mentoring me as I matured from an undergraduate to graduate student, researcher, and friend.

Special thanks go to Christian Davila for his detailed analysis on the thermoformed panel results, performing and collecting dating for the spectrometer experiment, and his effort in teaching me many technical things while inspiring a sense of humor and friendship within the group.

Special thanks go to Dae Wook Kim, who consistently inspired and motivated me to pursue great things, helped grow my passion for the field of optical sciences and engineering, and encouraged kindness, happiness, and excitement among myself and all my peers.

Special thanks go to Alex St. Peter, who led the experiments and documented the development of the custom chemical etching process, and who always worked with great enthusiasm and friendship.

Finally, special thanks go to all my close friends and family, who supported me unconditionally before and throughout my academic career.

Abstract

Astronomy is one of the most ancient fields in the natural sciences, with the subfield of radio astronomy emerging relatively recently by comparison. Despite this, radio astronomy has quickly grown to rival the older subfields of astronomy through its reputation to unravel new and fantastic discoveries about the Universe that were otherwise hidden in amongst the other wavelength bands. As each subsequent discovery seems to unveil further questions, the scientific goals aimed at answering them drive increasingly more extreme technological requirements, resulting in very difficult engineering and manufacturing challenges. With large-scale radio telescope observatories such as the next generation Very Large Array on the horizon, a more advanced, efficient, and cost-effective method of fabricating the panels that compose the telescope reflector surface is needed. In this report, I will summarize the research I have been involved in with the Solar Lab at the Department of Astronomy and Steward Observatory and the Large Optics Fabrication and Testing group at the James C. Wyant College of Optical Sciences, aimed at advancing radio and millimeter wave telescope panel fabrication. Specifically, I will discuss the development and testing of a novel adaptive freeform panel mold technology, and the investigation into a simple and effective panel surface treatment regime for solar scatter control.

Table of Contents

Chapter I.

Introduction

Since its inception, Astronomy has been a field that provides an endless stream of questions, wonder, and engineering challenges. The farther our technological prowess grows, the more questions we uncover, and the further they push us to define new ways to engineer systems that can answer them. Astronomy itself is the study of nearly everything around us, although more specifically it is a field aimed at understanding celestial bodies and phenomena. It is one of the oldest natural sciences, dating back to some of the earliest civilizations in recorded history, and has made significant and rapid advancements since the development of optical telescopes to aid in observational studies. While the development of optical telescopes for the purpose of astronomical observations has a history dating back over 400 years, a more recent advancement in the field is the emergence of a subfield now commonly known as radio astronomy.

Radio Astronomy and Telescopes

Radio astronomy is a subdivision within the field of astronomy dating back nearly 90 years, specifically focused on studying the cosmos through telescopes designed to operate in the radio wavelength range. The radio wavelength range is the portion of the electromagnetic spectrum ranging from roughly 1 mm to 1,000 km, or 1 THz to 10 KHz in frequency [1]. “Millimeter wave” refers to the range of frequencies within the broader radio spectrum that correspond to wavelengths on the scale of millimeters. Its inception occurred

when Karl G. Jansky constructed the first radio telescope while trying to solve a problem with interference in short-wave radio transatlantic communications in 1932 [2]. His work laid the foundation for the newly emerging field, and since then many different radio telescope systems have been constructed with increasing complexity and capability, allowing for astronomical discoveries that otherwise would not have been possible. The most recent and perhaps impressive example of this is the Event Horizon Telescope (EHT) which, consisting of an array of radio telescopes spread across the globe, was able to create the first ever image of a black hole in 2019 [3]. In addition to this, other advanced radio telescope observatories such as the next generation Very Large Array (ngVLA) are being proposed, which will have the capability to dramatically improve the current state of the art in both sensitivity and resolution for radio observatories, allowing for even more impressive discoveries to be made.

Fundamentally, radio telescopes take on a similar form to that of optical telescopes, with requirements equally similar. In general, high sensitivity, angular resolution, dynamic range, and spectrum coverage are all desirable, with tradeoffs made in the telescope design process to optimize the balance of these traits for the specific scientific requirements of the system. Because radio wavelengths are so much longer in comparison to optical wavelengths, diffraction effects lead the telescope angular resolution to be significantly worse than their optical counterparts for comparable aperture diameters. As a result, the primary reflector of a radio telescope tends to be significantly larger than that of even the largest optical telescopes, with aperture diameters over 10 m commonplace [4]. Another result of the longer wavelengths is a relaxation on the overall surface figure error requirements for the telescope mirrors when compared to high performance optical

telescopes. The required surface figure root mean square (RMS) error of the telescope reflector surface when compared to its desired shape is in the 10s of microns for millimeter wave operation, and grows increasingly larger for longer operational wavelengths [5]. Specifically, according to antenna tolerance theory, telescopes with a shortest operational wavelength of 1 mm require a reflector surface error smaller than 60 μm RMS error for optimal performance [6]. Due to the significantly larger surface figure error requirements and primary mirror diameters when compared with optical telescopes, the reflectors are typically made from multiple aluminum panels rather than a single glass substrate. These aluminum panels are individually shaped to be patterned together to approximate the full mirror surface. Often, this surface is either parabolic or hyperbolic due to the Cassegrain style design typical of most shorter wavelength radio and millimeter wave telescopes [1].

Panel Fabrication Techniques and Requirements

Historically, there are four main manufacturing techniques that have been used to fabricate the panels used for several prominent radio and millimeter wavelength telescopes, each with their own pros and cons. These include the techniques of machining, stretching, electroforming, and using carbon fiber reinforced plastic. While they are described in detail with context to the telescopes they have been used for in [6] and [7], I will provide only a short overview of the techniques as supplementary motivation for the main topic of the report. Machining involves taking a thick slab of material and incrementally removing material in a coarse milling process, followed by using grinding techniques to achieve higher precision. Stretching is a process by which a thin aluminum sheet is placed on a mold of the desired surface shape with holes connected to vacuum lines. Upon activating

the vacuum lines to hold the sheet against the mold, a glue is used to attach backup structure ribs with added weighting to keep them in place. After curing for several hours, the vacuum is released, and the aluminum sheet now approximates the desired surface and can be used as a panel. Electroforming is a process which starts by producing a negative mold where the reflective surface of the panel will be deposited. This mold is inserted into an electrolytic bath while a charge is induced, allowing the mold to serve as the anode in an electrolysis process. The cathode is a nickel blanket that is deposited onto the anode, creating a "skin" which replicates the mold shape and can be used as the reflective surface of the panel. Finally, carbon fiber reinforced plastic can be used to produce panels by laying it on a cast iron or glass mold. Upon producing two of these sheets with the same mold, they can be bonded to the top and bottom of an aluminum honeycomb core to form a rigid and usable panel, after applying a metallic layer to provide reflectance.

While each of the most common panel fabrication techniques described above can achieve surface figure RMS error values within the range of typical telescope requirements, they have specific downsides related to their cost, reusability, and efficiency for varied panel geometries. Specifically, machining panels individually requires an extremely large investment in both time and money, making it particularly unattractive for many radio telescope systems due to the numerous and varied panel shapes required for large dishes. Alternatively, the electroforming, carbon fiber reinforced plastic, and stretching methods all require a mold matching the desired surface shape of the panel for use in their respective manufacturing processes. Unfortunately, due to the often numerous and varied panel shapes making up the full reflector dish, this means many molds need to be acquired with highly accurate surface shapes before panel fabrication can take place, resulting in high

costs and time expended to machine or otherwise generate them. Additionally, once used, these often-expensive molds are rendered useless after the project is complete, unless another future design happens to require nearly identical panels.

As the demand for a high volume of radio and millimeter wave telescopes grows with large scale projects such as the next generation Very Large Array (ngVLA) and others drawing closer, more efficient, adaptable, and cost-effective panel fabrication processes become increasingly more important to support the growing science and engineering communities. In this report, I will summarize the ongoing research efforts made by the Solar Lab at the Department of Astronomy and Steward Observatory and the Large Optics Fabrication and Testing group at the James C. Wyant College of Optical Sciences to develop a technology and method of adaptive aluminum thermoforming for the fabrication of radio and millimeter wave telescope panels. I will first describe the work done to develop and test a novel adaptable mold technology with the potential to significantly reduce manufacturing costs for a high-volume production of varied panels. Following this, I will describe the related research that has been performed to investigate and demonstrate an easy to implement surface treatment regime for the panels to aid in solar scatter control. Finally, I will conclude with a summary of the results achieved so far, and a look ahead at future planned research.

Chapter II.

Adaptive Aluminum Thermoforming

This chapter will focus on the method of adaptive aluminum thermoforming for the fabrication of millimeter wave telescope panels. This process involves placing flat aluminum sheets on an adjustable freeform mold designed to approximate a particular surface shape designated for the panel, then heating up the whole setup in an oven until the panel gets hot enough to conform to the mold. Cooling the system back down yields panels which approximately match the surface figure shape of the mold. One of the limitations in the way that panel fabrication is typically carried out is that the mold used is typically not adjustable, which generally results in the need for a separate and unique mold to be machined for every nonidentical panel. As mentioned in chapter 1, this has the obvious effect of increasing costs and severely limiting reusability of the materials acquired to manufacture the panels. Another technical challenge is the phenomenon known as spring back, which describes the tendency for aluminum to relax back into its original pre-thermoformed shape by some non-trivial amount upon cooling, creating significant surface figure error [8]. This problem is an especially difficult one to deal with in the context of millimeter wave telescope panels, due to the relatively tight surface figure quality requirements that were discussed in the previous chapter.

In an effort to improve the panel manufacturing efficiency and characterize the spring back problem, a significant research effort has been poured into the development of an adaptable panel mold. By developing a mold that can change its surface shape to

approximate a range of different freeform curvatures, a single mold could be used to fabricate the panels for an entire millimeter or radio wave telescope dish, as long as the mold is of the appropriate size to account for the panel patterning geometry. This has the potential to greatly reduce panel fabrication costs and improve the manufacturing efficiency for the radio telescope industry. This technology can also be applied in other industries such as for satellite communication dishes and even architectural industries, however the driving motivation and focus for this report is on the benefits associated with radio telescopes. In addition to this, an adaptable mold has the potential to address the spring back challenge by providing a platform for detailed investigation into the phenomena.

Currently, there are very little if any literature resources available that describe the spring back phenomena fully in the specific context of radio telescope panel thermoforming, likely because it is a new and emerging manufacturing technique. It is also likely that the magnitude of the spring back effect depends on many variables, including the surface area of the panel, the thickness, and the concavity of the curvature(s) within the surface that is being approximated, further complicating the problem. An adaptable mold allows for these variables to be investigated by performing tests of adjusting the surface to approximate various shapes, thermoforming panels on the mold, and comparing the panel shape to the shape of the mold. This type of investigation facilitates the development of a predictive model to describe the spring back as a function of relevant panel parameters and could result in a fabrication procedure that involves setting the mold to a “pre-corrected” surface shape (different than the desired panel surface shape by some calculated and

specific amount), which will result in the thermoformed panel closely approximating the desired shape upon cooling.

Adaptive Freeform Mold

The Steward Observatory Solar Lab has been working on the development of a new technology that addresses the technical challenges described above, encompassing an adaptable mold with the ability to approximate different compound freeform curvatures to high accuracy and precision. While a description of the thermoforming process and a motivation for the adaptable mold was given above, in this section I will present an overview of the driving technology and features. I will describe how it works, the various prototype developments and changes made to the design, and the testing strategies and associated results accompanying each prototype. This testing incorporates both accuracy and precision/repeatability studies to characterize the adaptable mold prototype shaping capabilities and panel fabrication results.

The driving technology presented is an adaptable mold used to thermoform panels with varying compound freeform curvatures. This mold consists of several components that have undergone different realizations in three distinct prototypes that were designed, constructed, and tested in an effort to improve upon the previous design and performance. While each prototype is slightly different from one another, they all consist of a few prominent features. The first feature common to each prototype is a steel flexure sheet that can be described as a patterning of individual tiles, each connected to its neighbors via thin, deformable, spring-like members as depicted in figure 2.1. The second feature common to each prototype is an array of actuators connected to some (but not necessarily all) of these

tiles, which are controlled to move independently of one another in the vertical direction. By adjusting these tiles in piston, the compliance of their neighbors results in the centers to be set at the desired height, with slopes that vary, allowing for different curvatures to be approximated by the entire flexure surface when the actuators are adjusted to set the centers of the tiles to the heights corresponding to the desired surface. A two-dimensional drawing of these two features in a basic format demonstrates the how they work together to create an adjustable mold that can be used to approximate different surface curvatures [7].

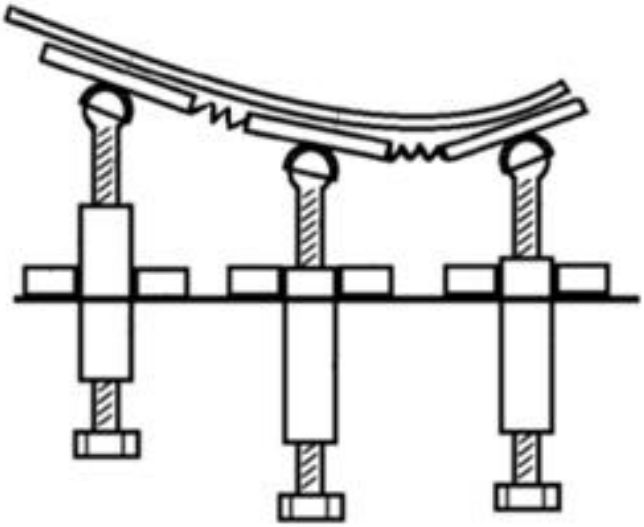

Figure 2.1. Adaptable Mold Concept Drawing

Adaptable mold concept drawing showing side view of actuator-driven shape deformation and panel conformation on top.

Prototype Adaptable Mold I

The first prototype realization of this concept that was assembled and tested consisted of a steel flexure composed of hexagonal tiles, where every tile was connected

from the back to a bolt which screwed into a steel backing structure. The size of the full flexure was 50 cm x 50 cm, for the purpose of thermoforming panels of about the same size. In this subsection, I will outline the key design features of the first prototype mold, the testing strategy and achieved results, and the technical challenges that appeared along the way.

Design Features

The hexagonal tiles composing the flexure surface were connected to each other with thin blade flexures on each side of the tile, which allowed them to change heights and slopes without deforming (assuming relatively small height changes). The back of each tile had a swivel where a steel a ball could snap into place, which was connected to a nut and could then be attached to the bolt actuator. Figure 2.2 shows a zoomed view of the back of the flexure before assembly, where the tile shape, blade flexures, and swivel-nut can be seen with a few bolt actuators connected.

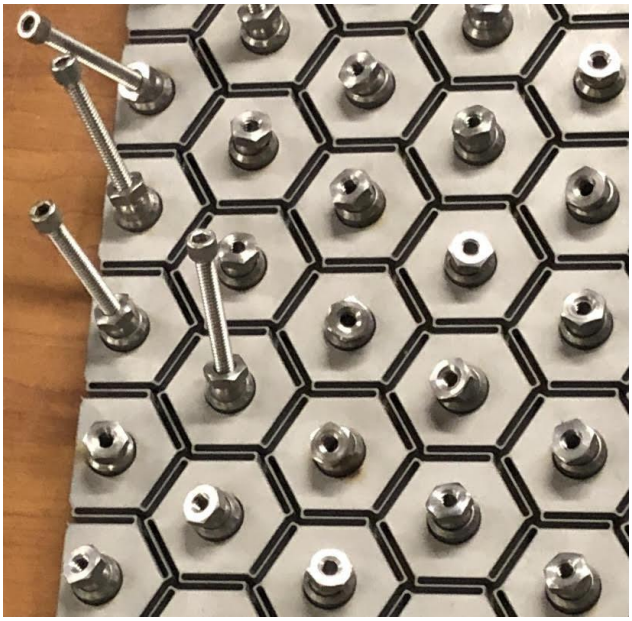

Figure 2.2. First Prototype Adaptable Mold Back Flexure

Zoomed view of the back of the flexure for the first adaptable mold prototype before assembly, with the swivel-nuts and several bolt actuators visible.

These bolt actuators connect to the back of the tile centers through the swivel-nuts, which through their rotation allow for the bolt actuator to maintain a purely vertical displacement upon adjustment, even as the tile's slope changes. The other side of the bolt is connected to a steel backup structure with holes inserted with threaded brass fittings, patterned to match the locations of the centers of each tile. An image of the back of the fully assembled first adaptable mold prototype is shown figure 2.3, to provide visualization of the backup structure.

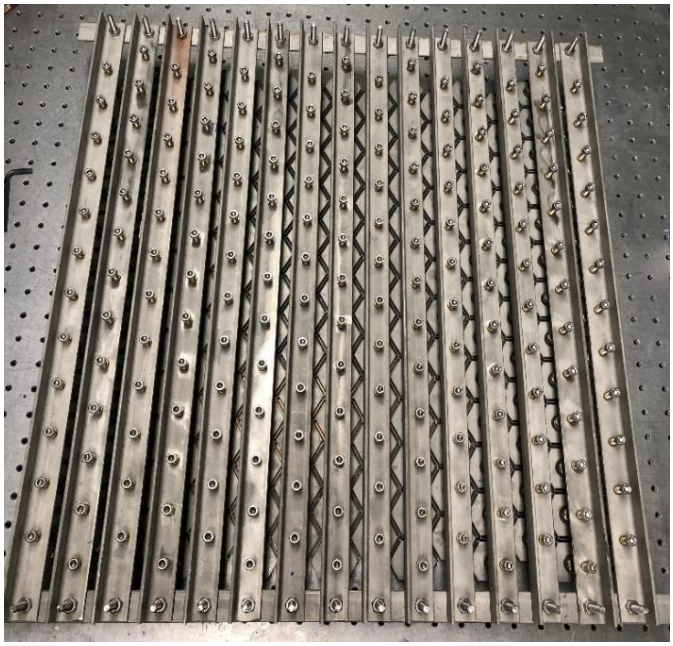

Figure 2.3. First Prototype Adaptable Mold Backing Structure

View of the backside of the fully assembled first adaptable mold prototype, highlighting the backup structure that connects the bolt actuators to the flexure.

The heights of these tiles could then be controlled precisely by adjusting these actuator bolts, and the distance that each bolt travels is directly dependent on the bolt rotation and thread pitch. A view of the fully assembled first adaptable mold prototype is shown in Figure 2.4, where the whole structure can be seen.

Figure 2.4. First Prototype Adaptable Mold

An alternate view of the fully assembled first adaptable mold prototype, showing the entire structure and flexure surface.

Testing Strategy and Results

After the construction of the mold was completed, we began testing its capabilities. Our primary goal in characterizing the mold shaping capabilities was to see how accurately

it could approximate a targeted surface shape. In order to accomplish this, we first had to choose an analytical surface equation to set the mold shape to. As the primary application for this mold is to fabricate millimeter wave telescope panels, we chose to set the mold shape to a paraboloidal section with a focal length of 2.5 m. The equation describing this symbolically is shown below:

$$f(x,y) = a(x^2 + y^2) + bx + cy + d$$

Where

$$a = \frac{1}{4f}$$

In this equation, f is the focal length of the paraboloid, and b, c and d are other fit parameters associated with the curve.

To set the mold shape, we developed an iterative process which involved measuring the mold surface with a CMM machine (one data point per tile center), fitting the point cloud data to the paraboloidal surface equation, and then calculating the residual error in the fit for each point/tile. The residual error for each data point was used to generate an array of distance values for each tile that would bring them to the location that perfectly satisfied the fit. These distance values were then transformed into the required degrees of rotation for each bolt actuator, and the adjustment process could proceed by rotating every bolt the specified amount, either counterclockwise or clockwise depending on whether the tile needed to move up or down. Once this was complete, the mold surface was measured again, and the process was repeated through multiple iterations until the RMS (Root Mean Square) error of the fit could no longer significantly decrease over the span of several

iteration cycles. The RMS error value of the measured data compared with the paraboloidal fit was therefore used as the primary metric for judging the shaping capabilities of the mold, and this value was recorded for each iteration. In figure 2.5, the RMS error vs iteration number is plotted with an exponential fit to show the trend upon shaping the mold to the shape described, where the lowest RMS error achieved was 54 microns.

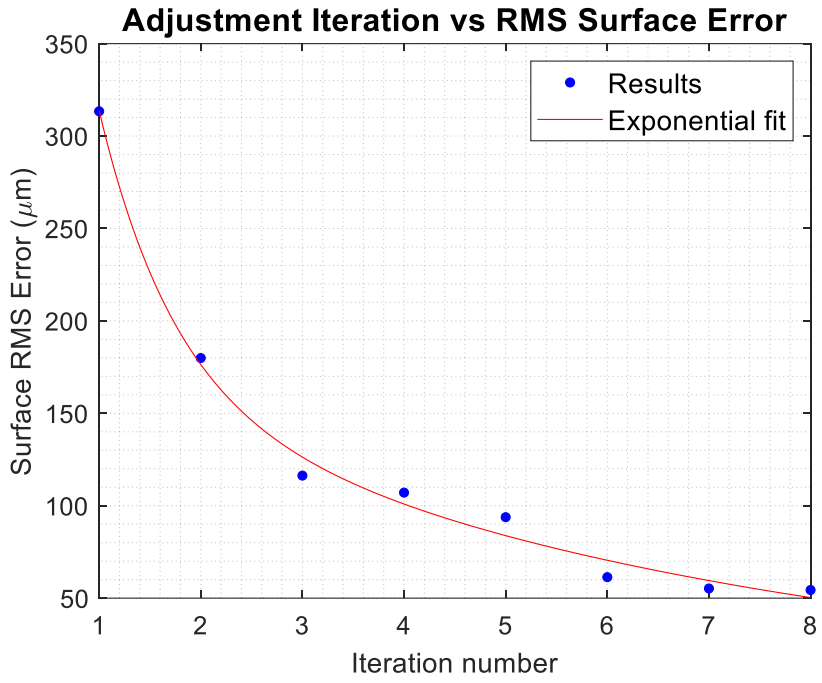

Figure 2.5. Mold Surface RMS Error vs Iteration Number

Adjustment iteration number vs surface figure RMS error for the first prototype adaptable mold shaped to a paraboloid with a 5m radius of curvature. The trend can be described with an exponential fit, bottoming out at 54 µm over 8 adjustment iterations.

Technical Challenges

One of the significant problems that developed with the first prototype adaptable mold was that the swivel nuts were adding some error to our adjustments due to the small

amount of “play” (space inducive of movement) between the swivel and the ball and connection, which resulted in bolt adjustments not immediately moving the tile upon rotation. This happened due to the bolt first travelling the distance in between the swivel and the ball before engaging with the tile. While the iterative nature of the adjustment process helped to mitigate the seriousness of this issue, it was problematic in how it increased the time it took to converge to a particular shape. Another problem was the fact that the adjustment had to be done from the back side of the structure. The result of this was that in practice, making mold adjustments comfortably required the entire mold to be tipped onto its side, and bolted into the optical table. Because the entire structure was made of steel it was very heavy, and we hypothesized that the self-weight deflection of the structure when propped onto its side was creating some issues in the adjustment of the bolt actuators due to the significant load it placed on them, and the increase in friction this induced when going through a rotation.

The most serious problem that developed which could not be resolved through multiple iterations, was the effect that the adjustment orientation (as described above) and thermal cycles had on the hardware elements of the mold. After the mold was put through multiple thermal cycles in the oven to thermoform panels, adjustments became much more difficult due to a growing inconsistency in the torque required to turn the bolts. Some bolts would require an immense amount of torque to turn, while others would require very little while not seeming to move the tile. The bolts that were difficult to turn induced galling between the threads connecting them to the swivel-nut due to the excessive friction being caused by the heavy load orientation of the adjustment setup. The bolts which were too easy to turn while not moving the tiles were a result of the brass fittings connecting them

to the backup structure becoming brittle over multiple thermal cycles. As the fitting became brittle, friction caused by rotating the screw would grind away the outer layer of material until it no longer fit within the holes of the backup structure, and instead spun freely without engaging with the bolt threads. These problems continued to worsen until the point that the mold became unusable and was eventually disassembled.

Prototype Adaptable Mold II

In an effort to improve the design of the adaptable mold and address the issues that were identified in the first prototype, a second prototype was developed that had several design changes. This prototype was smaller than the first prototype mold at 25 cm x 25 cm, to allow for cheaper experimentation and testing with the new design changes before committing to the larger size. In this subsection, I will outline the key design features of the second prototype mold, the testing strategy and achieved results, and the technical challenges that were discovered throughout the process.

Features and Design Changes

The first design change was oriented around the flexure. While the geometry associated with the flexure tile size and shape remained the same, instead of every tile being connected to an actuator, a pattern was chosen which cut their number down to about 30% of the number of tiles spread evenly over the entire flexure. This would significantly reduce the effort needed for the adjustment iterations, and the goal was to use this design to test if the same accuracy of the previous mold could be achieved. A more significant design change was that the flexure surface would be adjusted from the top rather than the bottom to allow for adjustment iterations to occur without ever changing the loading

orientation on the mold. This design change resulted in several other changes due to the implications it had on the mechanics of the mold. Rather than the bolt connecting from a backup structure to a swivel-nut attached to the back surface of the flexure, the bolt was instead attached from the top of the flexure surface by its head, where it passed down through a hole in the flexure and connected to a plate with threaded holes acting as a preliminary backup structure. A countersink was cut into the center of the top of the flexure tiles which had bolt actuators, to ensure the bolt head did not rise above the level of the top tile surface and interfere with the surface shape. In figure 2.6, a view showing a section of the top of the second prototype adaptable mold can be seen with access to actuator adjustment from the top of the flexure.

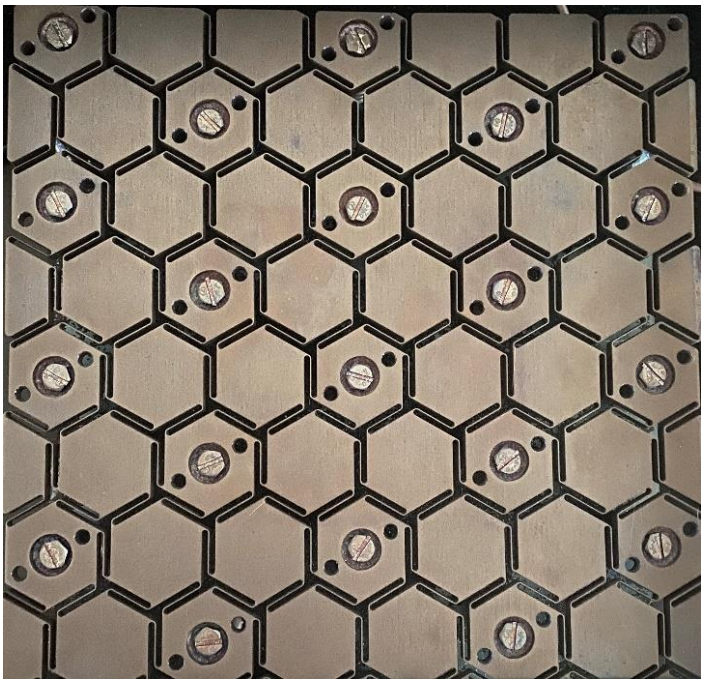

Figure 2.6. Second Prototype Adaptable Mold Flexure

View of the re-designed flexure on the second adaptable mold prototype, highlighting the reduced number of actuators, their patterning, and the ability to adjust them from the top.

With this design, there was no longer any component providing an upward force on the back surface of the flexure to ensure it was in contact with the bolt head, a problem that was prevented in the previous design by the swivel-nut constraining the connection between the flexure and the tile. Without this force, adjustments intending to increase the tile heights will not have any effect. In order to address this problem, a spring was chosen to fit around the bolt actuators in between the base plate and the back side of the flexure, with a spherical washer in between the top of the spring and the flexure. Upon assembling the mold, the flexure was tightened down onto the spring and spherical washer assembly using the bolt actuators. This caused the spring to be preloaded and provide an upward force on the back of the flexure, keeping it in contact with the bolt head upon further adjustment iterations. The spherical washer served a similar purpose to the swivel-nut from the previous prototype, allowing the spring to maintain an upward force on the back of the flexure while the tiles changed slopes. The material of the spring was selected to be Inconel, due to its strength retention properties under extreme thermal conditions. In figure 2.7, a side view of the prototype adaptable mold can be seen, emphasizing the addition of the spring and spherical washer components.

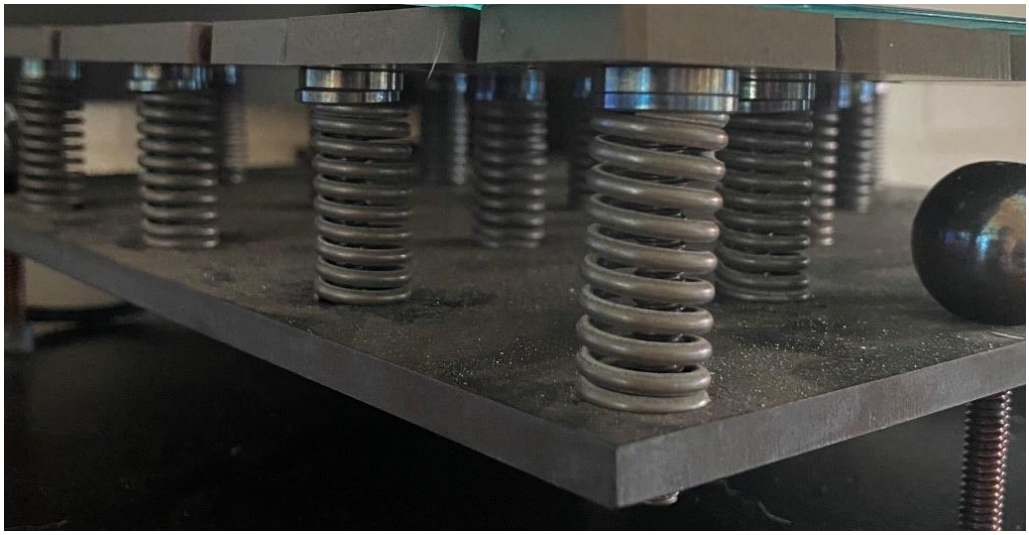

Figure 2.7. Second Prototype Adaptable Mold Spring and Washer Feature

Side view of a portion of the second adaptable mold prototype, highlighting the Inconel springs, spherical washers, and baseplate.

Testing Strategy and Results

The testing strategy for this mold was identical to the one used for the previous prototype mold. The primary difference was that instead of using a standard CMM machine, a portable CMM machine known as a FARO Arm was used for convenience. While the volumetric precision was less precise than the standard CMM machine previously used (±20 microns compared ±5 microns), the tool was sufficient for the extent of the testing done due to the RMS error values never dropping below the threshold. Similarly to the first prototype mold, the surface chosen to adjust the mold shape to was a paraboloid with a 2.5m focal length, described by the same equation shown in the previous subsection. The same iterative procedure described for the first prototype mold was used again here, and the results show a similar exponential trend of the RMS error dropping

over multiple iterations. In this case, the mold was able to reach a surface shape that matched the prescribed paraboloid with 45 microns of RMS error, slight improvement from the original design. Figure 2.8 shows the results of shaping the second prototype mold to the prescribed paraboloidal surface over several adjustment iterations.

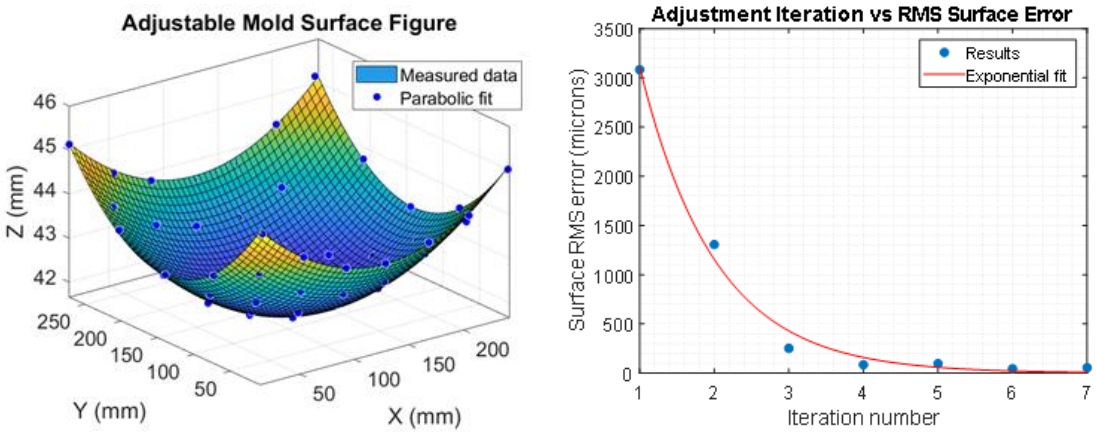

Figure 2.8. Second Prototype Adaptable Mold Shaping Results

Portable CMM point cloud data and paraboloidal surface fit for the second prototype mold best iteration (left). Adjustment iteration number vs surface figure RMS error for the second prototype adaptable mold, showing an exponentially decreasing trend bottoming out at 45 µm (right).

Technical Challenges

While the second prototype adaptable mold made significant improvements to the first, it was not entirely without its own problems and challenges. The main problem that was discovered throughout the testing process was the tendency for the bolt actuators to still have an inconsistency in the amount of torque required to adjust them. This problem became more apparent after the mold was subject to several thermal cycles during the testing process. While the shape was not greatly affected from the thermal cycles, further

adjustment of the mold became more difficult because some bolts suddenly became much harder to rotate, with one becoming entirely stuck. It was our belief that the galling problem discovered with the last prototype had not been solved, even though we had re-designed the mold to avoid unnecessary load on the bolts through the top-down adjustment approach. This discovery led us to believe that the thermal cycle itself played a role in this phenomenon, or at least contributed to an increase in the friction between the bolts and the threads.

Prototype Adaptable Mold III

The second prototype mold was meant to allow for the testing of new design concepts for the purpose of implementing some, if not all of them into a third prototype mold that would be of the same size as the first, with improved surface shaping capabilities. The results produced after assembling and testing the second prototype were promising because they showed it was able to achieve a slightly lower RMS error in about the same number of adjustment iterations, on a smaller scale with fewer actuators. Despite this, continual use of this mold after being subject to thermal cycles resulted in a variation of same problem present with the first prototype: bolts that became increasingly more difficult to turn.

Upon scaling up the second prototype into the third and most recent prototype mold, this problem was tackled by implementing a new design for the actuators controlling the tiles. Since the main issue with the previous prototype was caused by the bolts, a new design implementing steel cables as actuators in place of the bolts began development. The third prototype mold has been scaled back up to be 50 cm bx 50 cm and implemented many

of the same design choices that were developed for the second prototype mold, with the major change being the use of steel cables as actuators instead of bolts. As this prototype is still in the process of being developed, re-designed, and tested, the information presented is not complete, or equal in scope to that which was presented on the previous prototype.

Features and Design Changes

The third prototype mold design has retained several of the features that were present in the second prototype mold but increased in size back up to 50 cm x 50 cm and incorporated a key difference in the type of actuators used to drive the tiles. This mold was also constructed to sit within the center of the oven that is being used to thermoform the panels, to prevent having to move it in and out of the oven in between adjustment iterations and thermoforming sessions. As a result, portions of the oven frame were used to supplement the design. Rather than using bolts that were driven from the top down through the flexure into a baseplate, steel cables with ball bearings at each end will connect from the top of the flexure tiles to adjustable bolts attached to a steel bar beneath the mold base plate, outside of the interior of the oven. The same spring and spherical washer combination from the previous prototype will be used to provide upward preload force on the back surface of the flexure, however in this instance the cable passes through the spring as opposed to a bolt actuator.

Technical Challenges and Testing

While the introduction of cables to the most recent prototype design improves upon many design aspects present in the first and second prototype mold, it has seemingly introduced just as many new challenges and problems to solve. So far, the primary concern

is that the cables may stretch, inducing some non-linearity to the adjustment process. This issue will be tested by incrementally adjusting one of the bolts while measuring the corresponding tile displacement. This type of test will allow for the tile motion to be compared to the predicted motion defined by the thread pitch and bolt rotation, allowing for a determination of any non-linearities present in the adjustment system. At this point in time, these tests are still being performed and the results have not been summarized. The next step after performing this test will be to shape the mold to a surface similar (but not identical) to the one used for the first prototype, by incorporating the same iterative adjustment process. This will allow for a determination on whether the shaping capabilities can outperform the previous mold prototypes. The surface shape equation used to set the mold will not be identical to the one used in the first prototype to allow for an experiment on the thermal spring back phenomenon to take place. Details on what this study will entail and the reasoning behind the surface shape chosen will be explained in the next section, due to the background information necessary on the results of the thermoformed panels.

Thermoforming Procedure and Experimental Demonstration

In the previous section, the adaptable mold technology was detailed in the chronological order of its development. This broke down into three distinct prototype versions of the technology. Two of these prototypes have gone through a cycle of design, assembly, and testing. The third prototype mold is currently in the process of being re-designed, assembled and tested as new problems arise. The purpose of this section was to focus specifically on the features of the adaptable mold, the thought process and design challenges behind them, and the test results that support its performance and identify its

flaws. In this section, I will describe the results achieved using this technology to thermoform three separate millimeter wave telescope panels. Specifically, I will detail the thermoforming technology and techniques implemented, the resultant shape of the panels in comparison to the mold that was used, and the ideas on how to apply the gathered information to guide future fabrication processes that will further investigate and compensate for the spring back phenomena.

Thermoforming Technology and Procedure

While other thermoforming technologies are being explored, the one that was used to create the panels and results which will be presented in this report consisted primarily of a large oven controlled with a LabView program. The thermoforming procedure that we developed began by placing the adaptable mold in the center of the oven, centering the panel on top of the mold surface, and loading the top of the panel with a uniform and heavy weight. This weight consisted of a nearly 50 lb steel chain, coiled up to semi-evenly distribute the load across the panel surface. This was done to help ensure that the panel would conform to the shape of the mold upon heating up. We then closed the lid of the oven and controlled it to heat up at a linear rate until it reached 600 degrees Celsius. Two wire thermocouples were used to monitor the temperature in oven, with one set up to allow for estimation of the mold temperature and the other one reading the temperature of the air above the mold. Once the temperature of the mold reached 600 degrees Celsius, the oven would be controlled to maintain this temperature for approximately 1 hour. After this, it would be turned off entirely and left to cool at its own natural rate. Typically, it would take nearly 3-4 hours for the oven to reach temperature, and another 7-8 hours to cool back

down to room temperature. Once cooled, the panel was removed from the oven and measured.

Thermoformed Panel Results

So far, the only panels that have been thermoformed to a precisely prescribed shape with the adaptable mold technology was done so using the first prototype, after iterating it to its best shape. As described in the previous section, this was a paraboloid with a 5-meter radius of curvature at 54 microns of RMS error. Following the procedure described in the previous subsection, three 50 cm by 50 cm flat pieces of aluminum were thermoformed on the mold after being adjusted to this shape. These panels were all measured using the same CMM machine that was used to measure the mold. The results are summarized in table 2.1, showing the best fit paraboloid surface equation parameters, the focal length, and the RMS error values.

Table 2.1. Thermoformed Panel Results Summary

Fit Characteristics	Panel 1	Panel 2	Panel 3
Equation Parameters (mm): f(x,y) = a*(x^2+y^2)+b*x+c*y+d	a = -8.577e-05 b = 0.04093 c = 0.06863 d = -215.7	a = -8.684e-05 b = 0.04133 c = 0.06971 d = -216	a = -8.785e-05 b = 0.07218 c = 0.07481 d = -434.7
Focal Length (mm)	-2914.8	-2878.9	-2845.8
RMS error (μm)	85.32	88.32	88.19

The results from using the first prototype adaptable mold in its best shape to thermoform three panels are shown. The best fit parameters given the designated paraboloidal equation, focal lengths, and RMS errors are detailed.

The results achieved are promising, showing that three different thermoformed panels each achieved similar paraboloidal shapes with RMS errors less than 100 microns. Several other important things can be determined form the data. Firstly, all three panels have best fits to paraboloids with focal lengths longer than the paraboloid that the adaptable mold was shaped to. This effect is an example of the spring back phenomena that was described in the beginning of this chapter and provides a baseline for further experimentation to learn how to compensate for it.

To understand these results further, the best fit focal length for each panel can be averaged to define a mean focal length with additional statistics such as the standard deviation and variance. These results are summarized in table 2.2.

Table 2.2. Thermoformed Panel Best Fit Focal Length Statistics

Mean (mm)	Standard Deviation (mm)	Variance (mm)
-2879.8	34.5095	1190.9

The statistics of the best fit focal length for each of the three thermoformed panels is detailed, including the mean, standard deviation, and variance.

Using the mean focal length, an associated equation for the paraboloid that best characterizes all three of the panels can be defined. All three panels can then be fit to this

surface to estimate the repeatability of both the spring back effect on the panels, and thermoforming process itself. These results are displayed in table 2.3.

Table 2.3. Thermoformed Panel Results Fit to Mean Best Fit Focal Length

Fit Characteristics	Panel 1	Panel 2	Panel 3
Equation Parameters: f(x,y) = a*(x^2+y^2)+b*x+c*y+d	a = -8.6812e-05 b = 0.0414 c = 0.06948 d = -215.9	a = -8.6812e-05 b = 0.04132 c = 0.06969 d = -216	a = -8.6812e-05 b = 0.07133 c = 0.07393 d = -434.4
RMS error (μm)	89.51	88.1	91.64

The results obtained by fitting all three thermoformed panels to the equation for the best fit paraboloid defined by the mean best fit focal length are detailed, including the equation parameters and the RMS errors.

From this additional evaluation, it can be determined that the mean best fit focal length of all three panels was about 380 mm longer than the one prescribed to the mold shape at the time of thermoforming. This implies that the spring back effect increased the best fit the radius of curvature of the thermoformed panels in comparison to the best fit mold shape by a factor of 1.15. Additionally, the repeatability of this phenomenon was consistent, resulting in panels of the same shape with an RMS error difference between panels in the range of 3 microns. Finally, the overall surface fit of the panels to the mean focal length equation increased in RMS error by a consistent value of around 35 microns

compared to the RMS value fit to the mold shape. This implies that the spring back effect not only changed the panel surface shape by a repeatable ratio, but also consistently increased the RMS surface figure error of this shape in comparison to the mold shape.

Spring Back Considerations

The results summarized in the previous subsection are valuable and will allow us to establish the first few data points in the many more that will be required to fully characterize and compensate for the spring back effect in the future. Currently, our plan is to develop an algorithm that will allow us to determine the right shape to set the mold to that will result in thermoformed panels of a different desired shape. We will start with a simple linear model, by reducing the focal length of the paraboloid that the mold shape is set to by the same ratio that our results showed. Specifically, we will shape the third prototype mold to a paraboloid with a focal length that is reduced by the factor x/1.15, where x is the desired focal length of the paraboloid for the thermoformed panels. In this way, we are pre-compensating for the spring back effect to achieve panels of the desired shape. Of course, it is likely that this phenomenon is much more complicated and will also depend upon other factors in a non-linear fashion, including the focal length of the paraboloid, the size of the panel, and the RMS error of the mold shape. The third prototype mold will act as a tool to probe this phenomenon further and define an efficient algorithm to compensate for the spring back and fabricate panels of the desired surface figure with high precision and accuracy.

Chapter III

Surface Treatment Regimes for Solar Scatter Control

The previous chapter detailed the motivation, technology, and results achieved so far in the research area of adaptive aluminum thermoforming for millimeter wave telescope panel fabrication. This chapter will focus on a different but related area of research, focused on surface treatment regimes for millimeter wave telescope panels. This topic was of interest to the research team due to it being a necessary "finishing touch" required for most operational millimeter/radio wave telescope panels.

The motivation behind telescope designs incorporating surface treatments to their panels is to reduce the effect of specular reflected solar radiation on the telescope performance by controlling the surface roughness of the panels. One example of this being done is the ALMA (Atacama Large Millimeter/submillimeter Array) observatory, which has telescopes that incorporated chemical etching and rhodium plating treatments on their panels [9]. Surface roughness is a parameter that can play an important role in controlling the temperature gradients of the components that make up the telescope dish and its mechanical structure by the way it helps to control the surface reflectance. Temperature fluctuations have unwanted effects on the performance of the radio telescope due to the creation of thermally induced mechanical distortions on the secondary reflector surface shape [10], and/or potentially on the cryogenically cooled receiver system. The primary source of these temperature fluctuations is the sun itself, due to the large amount of radiance it produces and the fluctuating irradiance levels it imparts on the telescope as

environmental conditions change. The surface roughness parameter affects how diffuse or specular the panel surface is for incident solar radiation, which will determine the intensity of the radiation that is scattered onto other components such as the secondary reflector. If the surface roughness of a panel is increased from its baseline state of a few hundred nanometers RMS to the range of a few microns RMS using the appropriately designed surface treatment, the solar radiation will mostly scatter diffusely out and away from the dish over a large solid angle upon reflection [9], minimizing any heat energy concentrations or thermal gradients on the telescope components that would result from specular reflection.

In the context of panel fabrication, the next step after a panel is successfully thermoformed using the adaptive technology is to apply the appropriate surface treatment. As a result, the team became interested in understanding the requirements associated with these surface treatments, especially in relation to the surface roughness specification on the panels. With the development of custom treatment options that can be optimized for the individual panel purpose and be performed in the lab without outsourcing other facilities, the entire fabrication process can easily be performed with the technology developed by the research team, and optimized for the specific mission, science, or engineering requirements driving the purpose of the panels themselves. With this providing sufficient motivation to investigate the matter further, research was gathered on existing treatment techniques, leading to the modification of one common technique into a custom surface treatment procedure that was experimentally demonstrated and tested. This chapter will detail the development of the custom surface treatment so far and analyze its associated solar scatter efficiency in the context of millimeter wave telescope panels by incorporating

surface profile metrology data and experimental test results. While significant progress has been made, it should be made clear that this research effort is ongoing and the details in this report are only representative of the work which has been performed so far.

Custom Chemical Etching

The surface treatment regime that was developed was a modification of the type of treatment process known as chemical etching. Chemical etching is a process that involves applying a strong chemical etchant solution to remove unwanted portions of a workpiece material and is a technique that has been widely applied in machining practices. Several studies have been performed to characterize its effect on the surface roughness of workpieces composed of different materials, and with different etchant compounds [11]. For our process, we used an alkaline etching method that consisted of submerging an aluminum panel in a solution of caustic soda and distilled water. The caustic soda dissolves the aluminum over time, forming sodium aluminate and hydrogen gas. Concentration, time, and solution temperature can be varied to achieve unique surface qualities. A series of experiments were performed to explore these variables and arrive at an optimal etching process that achieves solar diffusivity within the range that meets the requirements for millimeter wave telescope panels.

To understand the effects of concentration percentage and time, we performed two tests. The first test involved fixing the concentration percentage of the solution and performing the process on several small sample aluminum workpieces for different increments of time. The second test involved the same procedure, however this time the submersion time was fixed, and the concentration percentage varied for several different

sample workpieces. In addition to this, the mass of each workpiece was measured before and after each etch for both tests, in order to understand how much material the process was removing. The results of these tests quickly showed concentration percentages higher than 30% created a chemical reaction that was too aggressive and removed too much material, on the order of 15% and larger. However, they also showed that lower concentration percentages did not yield noticeable differences in the appearance of the workpieces for lengths of time greater than 10 minutes. A separate test involving a spectrometer was used to measure the reflectance efficiencies of some of these samples to gain a better understanding of the subtle effects not noticeable by eye. Throughout this process, we estimated that a chemical concentration of 25% caustic soda to water, submerged over a timeframe of 10 minutes achieved the best results as estimated by visual appearance and measured surface RMS roughness. The result of applying this treatment recipe to a small sample panel is shown in Figure 3.1, where it is noticeable that the sample has a dull/diffuse appearance.

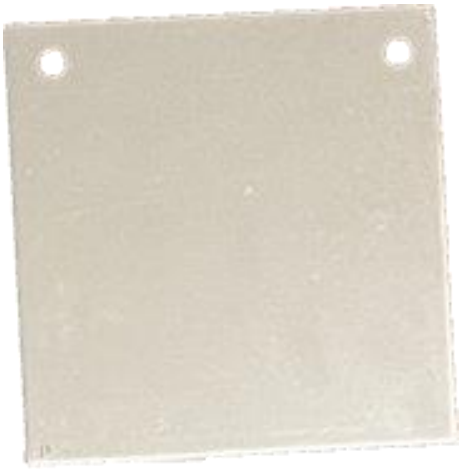

Figure 3.1. Chemically Etched Sample Aluminum Workpiece

Sample aluminum workpiece chemically etched with the estimated best recipe for solar diffusivity.

After determining that this recipe appeared to produce the best results visually, we had it measured with a profilometer to determine the surface roughness achieved and to provide a more quantitative estimation of the result in the context of solar scatter efficiency. We also had an untreated sample measured to better understand how much a treated sample was changed from its baseline state. Because we were interested specifically in the fine scale surface RMS roughness and the scan length was on the order of several centimeters, a polynomial fit was applied to and then subtracted from the data to remove any overall surface figure influence on the RMS roughness values that were calculated. The result of measuring an untreated sample is shown in figure 3.2, where the baseline RMS roughness was calculated to be 0.59 µm.

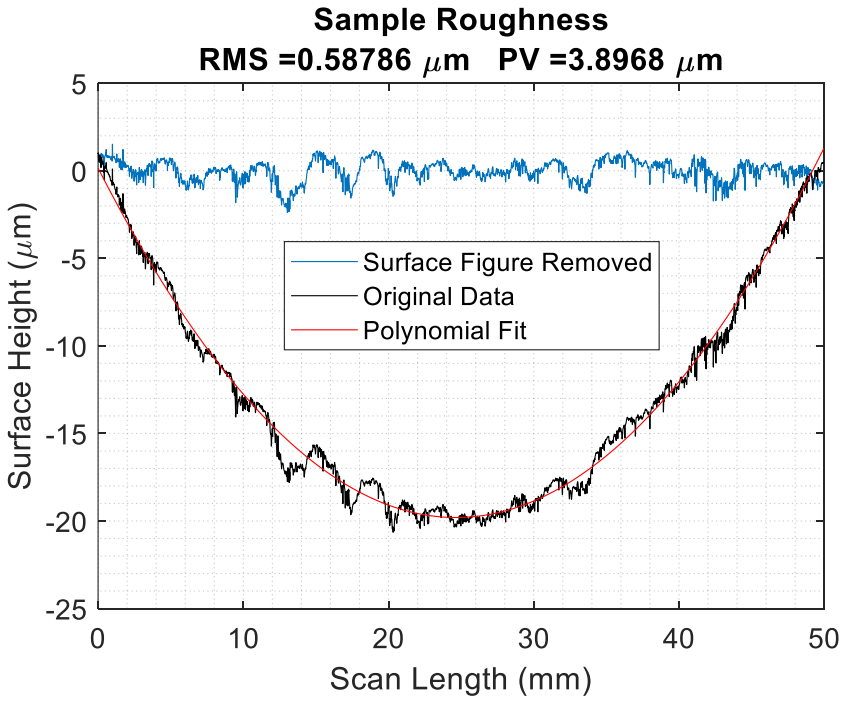

Figure 3.2. Surface Finish of Untreated Sample Workpiece

High resolution profilometer scan of an untreated sample panel, showing the surface height variation as a function of scan length with RMS and PV (peak to valley) parameters for the removed surface figure data listed. The original data (black), best fit polynomial (red), and removed surface figure data (blue) are all plotted.

The result of measuring a different sample that was treated with the estimated best chemical etching recipe is shown in figure 3.3, where it can be seen that the process succeeded in increasing the surface roughness to 1.7 µm RMS.

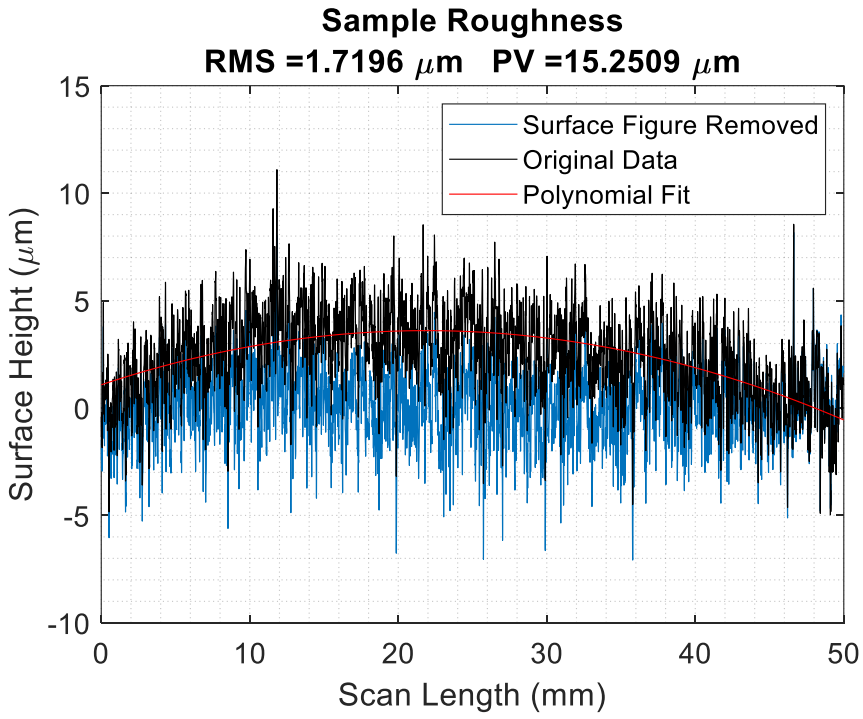

Figure 3.3. Surface Finish of Chemically Etched Sample Workpiece

High resolution profilometer scan of the sample chemically etched with the optimal recipe, showing surface height variation as a function of scan length with RMS and PV (peak to valley) parameters for the removed surface figure data listed. The original data (black), best fit polynomial (red), and removed surface figure data (blue) are all plotted.

Because these measurements were performed on two separate samples rather than the same sample before and after treatment, it does not give a perfect representation of relative increase in RMS roughness. Despite this, with the assumption that all untreated samples are similar to each other in surface finish, we can still see the effect of the treatment. With knowledge of the surface roughness, the ratio of specular to total reflected radiation can be estimated using the equation shown [12]:

$$\frac{R_s}{R_t} = e^{-\left(4\pi\frac{\sigma}{\lambda}\right)^2}$$

where Rs is the specular reflectance of the rough surface, Rt is the reflectance of a perfectly smooth surface of the same material, σ is the surface RMS roughness, and λ is the radiation wavelength. For example, a reasonable requirement for millimeter wave telescope panels is to achieve at least 98% of specular reflection at the minimum observational wavelength (λ = 1 mm). For this surface treatment regime, the measured surface roughness (σ = 1.72 μm) will be 99.95% specular for this wavelength, and approximately 0% specular at a benchmark wavelength (i.e., $\lambda_{benchmark}$ = 5 μm) in the solar spectrum. It should be understood that the equation above describes only the specular component of the reflected radiation, and not the total reflected radiation. In general, the total reflected radiation along any direction is determined by both specular and diffuse components, which are functions of the surface RMS roughness and surface RMS slope irregularities, respectively. While the total reflected radiation can be estimated as being composed entirely of one or other (specular or diffuse) components depending on whether the wavelength is significantly large or small compared to the size of the surface features [12], this is not particularly important for our estimations. Because the greatest concentration of energy that could

induce significant distortions on the telescope mirrors is present in the specular component of the reflected radiation only, we are primarily concerned with determining how specular *or* diffuse the panels are in the solar spectrum, rather than determining the total reflection along any specific direction. Assuming that the scattering efficiency is represented by the diffuse component of the reflected radiation, knowledge of the surface roughness of a sample panel allows for an estimation of the solar scattering efficiency achieved by the surface treatment through the means of calculating the specular reflectance efficiency. This estimation also provides a useful reference for the experimental test results described in the next section.

Spectral Specular Reflectance Testing

In addition to exploring the different parameters involved in the chemical etching process and measuring the resulting surface roughness parameters to provide estimates of the solar scattering efficiencies, experimental measurements were also performed. While measuring the specular reflectance of the samples in isolation proved to be difficult with the equipment available, an experiment was still setup that allowed for measurement of the total reflectance along the specular direction for the test samples. This experiment allowed us another means of estimating how well wavelengths falling within the peak solar irradiance range are efficiently scattered when varying controllable parameters in the etching process. Since solar irradiance peaks in the visible spectrum, an experimental setup was designed using a tungsten halogen light source to simulate a solar source, and a compact spectrometer to measure the spectral reflectance along the specular direction of samples with different surface treatments over the range of 400 – 1000 nm. Tungsten

halogen light sources have been used frequently for solar simulations because of their availability, usability, low cost, and similar spectrum and spectral interval to the sun. It is not a perfect match however, due to the fact that tungsten halogen lamps radiate at a temperature lower than the sun, shifting the approximate blackbody curve further towards the infrared in comparison [13]. Despite this, it was determined to be similar enough to extract meaningful data for purpose of our experiment. Specifically, we used a tungsten-halogen light source from StellarNet Incorporated for our experiment, with a spectral range of 350 – 2200 nm. The spectrometer used was a compact CCD spectrometer from Thorlabs with an operational wavelength range of 200 – 1000 nm. A Thorlabs fiber bundle optimized for use with spectrometers created a single cable solution to connect the spectrometer, light source, and sample for reflection spectroscopy. This fiber bundle solution is shown in figure 3.4, where once connected, the 6 outer fibers distribute the source light to a lens adaptor which focuses it down onto the sample. The light reflected from the sample passes back through the lens, where it is focused into the central fiber that connects to the spectrometer.

Figure 3.4. Fiber Bundle and Adaptor

Image of the fiber bundle and adaptor used to connect the light source and spectrometer into a single cable, providing an easy solution for obtaining approximate spectral specular reflectance data for the sample panels. The left figure shows a side view of the bundle, and the right figure shows a view looking into the adaptor aperture with the light source shining through.

The experimental setup is shown in figure 3.5, with the light source, spectrometer, and samples labeled. With the instruments on and connected, the aperture of the fiber bundle tip adaptor was placed flat, directly over the centers of the sample panels to collect the spectral data for reflection along the specular direction.

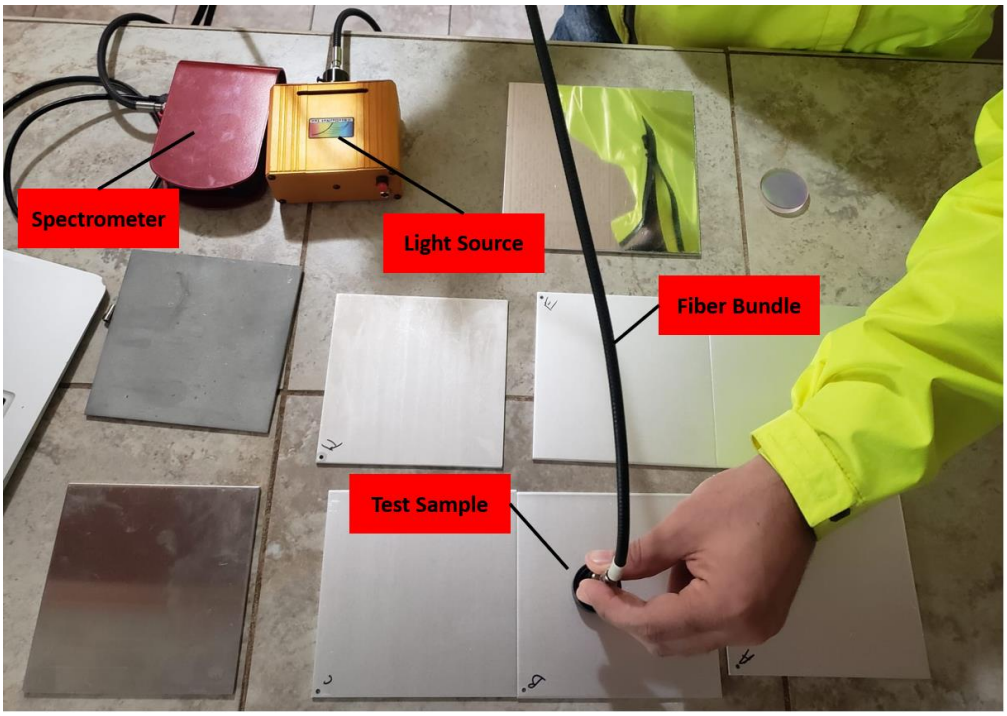

Figure 3.5. Spectral Specular Reflectance Experimental Setup

Image of the experimental setup for the spectral specular reflectance experiment, showing the spectrometer, light source, fiber bundle, test samples, and measurement method.

Shown in figure 3.6 are the results obtained from this experiment, specifically comparing the reflection efficiencies along the specular direction of four chemically etched panel samples that were treated with the same chemical concentration over different lengths of time, as well as an untreated and polished sample for reference. The y-axis of the plots were normalized by the reflected irradiance values from the untreated sample.

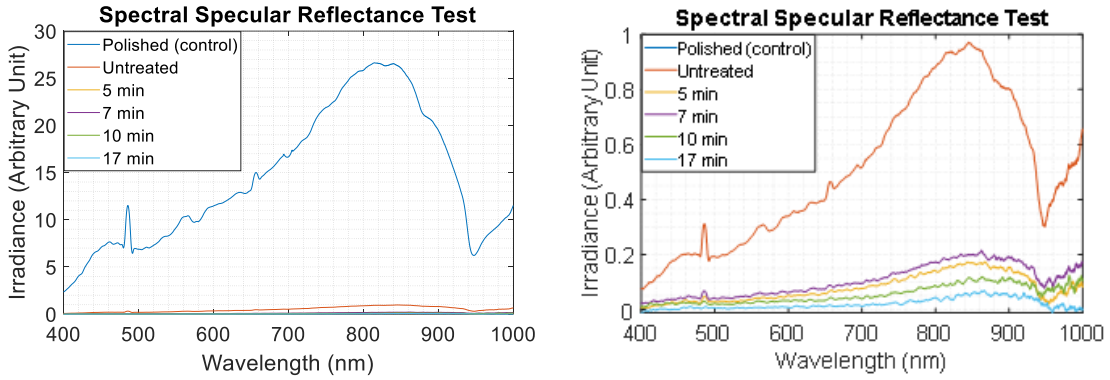

Figure 3.6. Measured Spectral Specular Efficiencies for Different Sample Treatments

Spectrometer measurement results showing specular reflectance efficiency as a function of wavelength for panel samples treated with the same chemical concentration over different lengths of time. The right plot shows a zoomed view of the left with a reduced y-axis limit.

While none of the panel samples shown in these results were treated with the estimated best etching recipe, they do clearly communicate some information about the effectiveness of process in general. The first point worth noting is that all treated samples have spectral reflectance efficiencies significantly reduced from the untreated panel, with the shortest treatment time resulting in a reflectance drop of nearly 80% at the peak wavelength. The second point is the fact that there is a clear trend visible, showing that an increase in treatment time decreases the reflectance efficiency. Finally, it should be pointed

out that this experiment does not provide a true representation of spectral reflectance efficiencies in isolation, due to the fact that some of the diffuse component of the reflected irradiance will lie along the specular direction. Additionally, the experimental setup only allows for an approximation of how panels with these treatments will respond under actual sunlight, since the source used was not the real sun. Regardless, because the test still encompasses the peak spectral range of transmitted solar irradiance and also shows only relative reflectance values for treated samples compared specifically with an untreated sample, it still provides a useful tool for understanding the effectiveness of the treatment for increasing solar scattering efficiency. With these preliminary studies completed, future development of the optimal treatment regime can be accomplished, supplemented by additional experimentation.

Chapter IV

Future Work and Conclusions

This report acts as a summary of the ongoing research effort being performed by the Department of Steward Observatory and the James C. Wyant College of Optical Sciences, specifically involving the Steward Observatory Solar Lab and the Large Optics Fabrication and Testing Group. This effort is primarily motivated to aid in the advancement of radio and millimeter wave telescope panel fabrication, by developing a novel technology that has the potential to greatly improve the efficiency and required costs that are associated with the manufacturing process. In chapter 1, I provide a brief introduction to radio astronomy, telescopes, and the historically accepted and used panel fabrication methods, with the purpose of providing motivation for the necessity to advance these methods as the demand for a high volume of radio telescope antennas grows with the next generation of radio telescope observatories on the horizon. In chapter 2, I introduce the adaptable mold technology that is being developed by the Steward Observatory Solar Lab and specifically detail the work I have been involved in to construct and test two prototypes, showing promising results and a strong foundation for future study and development. In chapter 3, I detail the related work I have been involved with to create a simple surface treatment strategy incorporating a chemical etching process that can be applied to the thermoformed panels for the purpose of increasing their solar scatter efficiency. The foundation of this report is built on the two recently submitted and accepted Optical Society (OSA) summary publications for the 2021 Optical Design and Fabrication Congress [14,15].

While I have been fortunate enough to be involved in a significant portion of this work, as research often goes there remains an even greater amount of future work to be done to develop these technologies before they can be applied in a mass production setting to serve the greater science and engineering communities. As shown in chapter 2, the first prototype of the adaptable technology was shaped to a paraboloid with a focal length of 2.5 m to an accuracy of 54 μm RMS error, and resulted in thermoformed panels of a slightly different shape with an accuracy of about 89 μm RMS error. Impressively, these results are not far from the requirements established for effective millimeter wave telescope operation, as described in chapter 1. However, they also exposed the magnitude of the problem of thermally induced spring back, which will be a topic for future study. Improvements were made to this technology to generate the second prototype, and the third prototype is currently in development. The specific goals for the most recent prototype are for it to have a shaping capability that outperforms the previous two in terms of accuracy and variability, and to use it to establish a spring back algorithm that can allow calculation for compensating the mold shape to produce panels that have the desired best fit surface, with an RMS error lower than what was previously achieved. Additional future work is also planned to scale up the size of the mold to have the capability to fabricate panel sizes near 2 m x 2 m, and to investigate a new electromagnetic thermoforming process detailed in [7]. Finally, additional work is also planned for the development of the panel surface treatment strategy. While an estimated optimal chemical etching recipe was established and measured as described in chapter 3, additional study needs to be done to better understand how the process may affect the overall surface figure of a panel shaped to high accuracy.

Additionally, the specific procedure still needs to be detailed, streamlined, and scaled to work for panels significantly larger than the small samples that have been currently studied.

Even with many more hurdles to surpass, the results achieved in these areas by the two departments at the University of Arizona provide a strong foundation for the future development of revolutionary radio telescope technology and symbolize a promising step for the future of astronomy, science, and engineering as a whole.

References

[1] J. Cheng, “Fundamentals of Radio Telescopes,” in *The Principles of Astronomical Telescope Design*, J. Cheng, Ed. New York, NY: Springer, 2009, pp. 339–376.

[2] J. W. M. Baars and H. J. Kärcher, “Birth of Radio Astronomy,” in *Radio Telescope Reflectors*, vol. 447, Cham: Springer International Publishing, 2018, pp. 31–61.

[3] K. Akiyama, “First M87 Event Horizon Telescope Results. I. The Shadow of the Supermassive Black Hole,” *The Astrophysical Journal Letters*, p. 17, 2019.

[4] J. W. M. Baars and H. J. Kärcher, “Evolution of the Telescope,” in *Radio Telescope Reflectors: Historical Development of Design and Construction*, J. W. M. Baars and H. J. Kärcher, Eds. Cham: Springer International Publishing, 2018, pp. 9–30.

[5] J. Cheng, “Millimeter and Submillimeter Wavelength Telescopes,” in *The Principles of Astronomical Telescope Design*, vol. 360, New York, NY: Springer New York, 2009, pp. 443–499.

[6] J. W. M. Baars and H. J. Kärcher, “Emergence of Millimetre-Wavelength Telescopes,” in *Radio Telescope Reflectors: Historical Development of Design and Construction*, J. W. M. Baars and H. J. Kärcher, Eds. Cham: Springer International Publishing, 2018, pp. 107–152.

[7] C. Davila-Peralta., “Electromagnetic Thermoforming to Manufacture Reflective Panels for Radio Telescopes and Downlinks,” *2021 IEEE Aerospace Conference*, 2021.

[8] H. Laurent *et al.*, “Mechanical Behaviour and Springback Study of an Aluminium Alloy in Warm Forming Conditions,” *ISRN Mechanical Engineering*, vol. 2011, Apr. 2011.

[9] J. W. M. Baars, “Reflectivity, scattering and emissivity measurements on samples of prospective ALMA reflector panels,” ALMA Memo 566, 2006.

[10] D. Chen, H. Wang, H. Qian, G. Zhang, and S. Shen, “Solar cooker effect test and temperature field simulation of radio telescope subreflector,” *Applied Thermal Engineering*, vol. 109, pp. 147–154, Oct. 2016.

[11] O. Çakır, “Chemical etching of aluminium,” *Journal of Materials Processing Technology*, vol. 199, no. 1, pp. 337–340, Apr. 2008.

[12] H. E. Bennett and J. O. Porteus, “Relation Between Surface Roughness and Specular Reflectance at Normal Incidence,” *J. Opt. Soc. Am., JOSA*, vol. 51, no. 2, pp. 123–129, Feb. 1961.

[13] E. Yandri, “Uniformity characteristic and calibration of simple low cost compact halogen solar simulator for indoor experiments,” *International Journal of Low-Carbon Technologies*, vol. 13, pp. 218–230, Sep. 2018.

[14] Z. Hatfield, “Adaptive Aluminum Thermoforming for Precision Millimeter Wave Telescope Panels,” *Optical Design and Fabrication Congress* (to be published).

[15] Z. Hatfield, “Surface Treatment Regimes for Solar Scatter Control in Millimeter Wave Telescope Panels,” *Optical Design and Fabrication Congress* (to be published).